Available online at www.sciencedirect.com

ScienceDirect

Journal of Magnesium and Alloys 6 (2018) 121–133

www.elsevier.com/locate/jma

Full Length Article

# Effects of cold and warm cross-rolling on microstructure and texture evolution of AZ31B magnesium alloy sheet

Litzy Lina Choquechambi Catorceno[a,*], Hamilton Ferreira Gomes de Abreu[a], Angelo Fernando Padilha[b]

[a] *Department of Metallurgical and Materials Engineering, Federal University of Ceará - UFC, Campus do Pici - Bloco 729, CEP 60440-554 Fortaleza, CE, Brazil*

[b] *Department of Metallurgical and Materials Engineering, Polytechnic School, University of São Paulo – USP, Av. Professor Mello de Moraes, 2463, CEP 05508-030 São Paulo, SP, Brazil*

Received 18 November 2017; received in revised form 20 April 2018; accepted 23 April 2018
Available online 26 May 2018

**Abstract**

Mg alloys conventionally rolled often present strong basal textures that affect negatively further deformations, limiting their applications. The present research found that cross-rolling experiences in adequate conditions can weaken those intense basal textures as a result of the interaction of deformation mechanisms and dynamic recrystallization. The effects of rolling temperature and strain rate on the microstructure and texture of an AZ31B magnesium alloy sheet generated heterogeneous microstructure where the initial basal texture was strengthened during cold cross-rolling and it was gradually weakening by the rolling reduction and the rolling temperature increases in such a way that a rather weak basal fiber was produced applying reductions higher than 15% at temperatures higher than 200 °C. Their ODF functions supported the texture weakening, exhibiting a combination of two crystallographic orientations represented by $\{0001\}<2\bar{1}\bar{1}0>$ and $\{0001\}\langle 10\bar{1}0\rangle$.


*Keywords:* AZ31B magnesium alloy; Microstructure; Texture; Cross rolling.

## 1. Introduction

Wrought magnesium alloys, in the form of sheets, have recently increased in popularity to be used as semi-finished products by the automotive and aircraft industries in the manufacture of lightweight and rigid components, such as inner door panels, engine bonnets, roofs, fenders and seat components, which were commonly produced as cast materials [1], although some makers of portable electronics have already successfully used wrought magnesium alloys sheets to manufacture computer housing and mobile phone and camera cases, since they offer an acceptable heat dissipation capacity. The growing interest in wrought magnesium alloys is due to their high specific strength, low density (~0.0018 Kg/m$^3$) and high stiffness that make them attractive for the production of lightweight structures [2]. The industrial-scale manufacture of magnesium alloy sheets is commonly from cast slabs, using either consecutive multi-pass hot rolling processes combined with intermediate annealing treatments or twin-roll casting technologies, which manufacture large thin plates of uniform thickness (<5 mm) directly from their melts [3]. Cold rolling is rarely employed in industrial-scale because these alloys possess poor ductility and high anisotropy at low temperatures restricting the deformability and generating edge cracks when the rolling reduction is greater than 10% [4]. Their limited ductility at low temperatures is related to the symmetry of hexagonal close-packed structure (HCP) of magnesium alloys, which offers an insufficient number of deformation modes at low temperatures. According the von Mises criterion, it is necessary at least five independent slip systems in a polycrystalline material to develop homogeneous plastic

* Corresponding author.
*E-mail address:* litzy222@yahoo.es (L.L.C. Catorceno).

https://doi.org/10.1016/j.jma.2018.04.004

deformation by crystallographic slips, however the two independent slip systems of HCP structures are insufficient to fulfill the von Mises requirement [5]. Thus, mechanical twins are activated as additional deformation modes to enable plastic deformation, generating abrupt crystallographic reorientations between the twinned region and the magnesium matrix, which in turn can facilitate further deformation modes and modify the crystallographic texture [6]. In contrast to them, non-basal slips generate only small gradual lattice reorientations but contribute more to deformation; however, it is difficult to activate them at low temperatures due to their high critical resolved shear stresses (CRSS), which are temperature dependent, gradually decreasing their values with the rolling temperature increases [5].

The mechanisms involved during deformations below the recrystallization temperature (cold rolling) of magnesium alloys include basically basal slips and mechanical twins formed preferentially on pyramidal systems ($\{10\bar{1}2\}<10\bar{1}1>$ and $\{10\bar{1}1\}<10\bar{1}2>$) [7]. However, above the recrystallization temperature, the dynamic recrystallization occurs simultaneously with the deformation mechanisms, producing recrystallized grains associated with twinning and secondary phases. In this regard, mechanical twins play an important role during deformation, affecting directly the strengthening mechanisms, texture evolution, asymmetric stress–strains and fracture initiations [8]. Their contributions to the evolution of texture and microstructure depend on the type of mechanical twins generated during deformation, which is controlled by the applied stress field and the grain size. Magnesium alloys with fine-grains ($<10\,\mu m$) inhibit twinning formation, promoting the activity of non-basal slips and grain boundary sliding, even at low temperatures [9].

The $\{10\bar{1}2\}$-extension twins, $\{10\bar{1}1\}$-contraction twins and double twins are frequently reported during the magnesium alloy deformations, the activation of each one of them is associated to specific strain path, such as the activation of $\{10\bar{1}2\}$-extension twins is developed under tensile loads applied parallel to the c-axis of the lattice, providing an elongation along the c-axis of the matrix and lattice re-orientation (~86°) about the $<11\bar{2}0>$ direction. In contrast, $\{10\bar{1}1\}$-contraction twins are generated during compressive loads applied parallel to the c-axis, which provide contraction strains along the c-axis, reorienting the basal planes ~56° about the $<1\bar{2}10>$ direction [10,11]. In the case of double-twins, they are formed from compression twins, which are twinned again by tensile twins forming orientations about 30–45° with respect to ND. Lentz et al reported that double twins have been correlated to void and crack formation and flow localization in the vicinity of twin boundaries; consequently several studies try to reduce or suppress their development with rare-earth alloying or grain size reduction. The exact misorientation of twins is strongly associated with c/a ratio that is close to the ideal value (~1.624) for magnesium alloys and can be slightly altered by alloying and thermo-mechanical treatments [1].

Most deformation processes generate extension twin due to their lower CRSS values (2–3 MPa) compared to the CRSS of contraction twins (between 30 and 100 MPa) [12]. It was found that extension twins enhance the uniform elongation during low strain rates; whereas high strains generate massive formations of extension twins, which can contribute to premature failures because their twin boundaries act as strong barriers for further dislocation slip, generating high dislocation pile–ups, work hardening and high localized stress concentration in such a way that cracks are initialized easily [13,14].

On the other hand, most deformation textures in wrought magnesium alloys are commonly associated to mechanical twins, since their strong basal texture is a direct consequence of deformation modes active during their manufacture, while pointing out that a strong basal texture negatively affects the mechanical properties and further plastic deformations, especially at low temperatures, enhancing the anisotropy levels, and remaining almost unchanged after heat treatments [15,16]. For this reason, numerous studies are being developed in order to find out deformation methods able to weaken the strong basal texture of magnesium alloys. Chino et al. and Zhang et al. found that the cross-rolling process can weaken or strengthen the basal texture via the simultaneous activation of different deformation modes [28]. The changes in deformation paths and shear deformation direction significantly affect on the microstructure evolution, residual stress distribution, directional dependency of mechanical properties more than conventional unidirectional rolling [17,18]. Therefore, a cross-rolling process under suitable conditions can weaken the basal texture of wrought magnesium alloy sheets, especially when the rolling temperature is carefully selected to facilitate the metal flow and reduce the load requirement [13]. In this regard, the main aim of the current work is to study the effects of rolling temperature on the microstructure and texture evolution of cross-rolled samples deformed at various rolling temperatures with different thickness reductions. A complete understanding of the microstructure characteristic and texture evolution of magnesium alloys subjected to plastic deformation represent an important tool to predict and control manufactured specimen quality, and help to identify adequate processing conditions, such as rolling temperature, rolling speed, deformation degree and their effects on the final microstructure.

Table 1
Chemical composition of the AZ31B magnesium alloy sheet.

| Chemical composition (in % mass fraction) | | | | | | |
|---|---|---|---|---|---|---|
| Material | Mg | Al | Zn | Mn | Si | Cu |
| AZ31B | Balance | 2.38 | 0.20 | 0.22 | 0.05 | 0.005 |

### 1.1. Experimental part

The material used in this research was a 2 mm thick commercial AZ31B magnesium alloy sheet produced by twin-roll casting, the chemical composition of which is presented in Table 1.

Table 2
Experimental conditions of cross-rolling experiences.

| Final thickness mm | Thickness reduction % | Rolling temperature °C | True strain Ɛ | Strain rate $s^{-1}$ |
|---|---|---|---|---|
| 1.9 | 5.5 | 25 | 0.06 | 1.31 |
| 1.8 | 10.0 | 25 | 0.11 | 1.81 |
| 1.7 | 15.0 | 25 | 0.16 | 2.28 |
| 1.9 | 5.5 | 100 | 0.06 | 1.31 |
| 1.8 | 11.0 | 100 | 0.12 | 1.91 |
| 1.7 | 15.5 | 100 | 0.17 | 2.33 |
| 1.8 | 11.0 | 200 | 0.12 | 1.91 |
| 1.7 | 15.5 | 200 | 0.17 | 2.33 |
| 1.8 | 15.0 | 250 | 0.16 | 2.28 |
| 1.7 | 20.0 | 250 | 0.22 | 2.71 |
| 1.6 | 25.0 | 250 | 0.29 | 3.10 |
| 1.6 | 20.0 | 300 | 0.22 | 2.71 |
| 1.4 | 30.0 | 300 | 0.36 | 3.54 |
| 1.2 | 40.0 | 300 | 0.51 | 4.39 |

In order to change the rolling direction of the as-received material, small strips of $10 \times 60$ $mm^2$ were cut from the twin roll-caster sheet in such a way that their long side was kept perpendicular to their original rolling direction. Thus, all cross-rolling experiences were carried out in a single pass by simply changing the rolling direction of the as-received material, and increasing gradually their thickness reductions until the maximum rolling reduction had been reached for each rolling temperature (25 °C, 100 °C, 200 °C, 250 °C and 300 °C).

All rolling reductions were carried out on a laboratory rolling mill with a roll diameter of 108 mm, applying a rolling speed of 0.056 m/s. The experimental conditions are shown in Table 2.

The microstructure characteristics and texture evolutions were examined on the rolling surface of deformed samples using complementary techniques, including X-ray diffraction (XRD), optical microscopy (OM) and scanning electron microscopy (SEM) equipped with an X-ray spectrometer (EDX). For metallographic analysis, small specimens were ground through different series of silicon carbide waterproof papers (400, 800, 1200, 2500 and 4000 in ANSI/CAMI grit size scale) and polished with 1 μm diamond suspension. Twins and grain morphology were revealed using two etching solutions: a first solution (10 ml nitric acid, 30 ml acetic acid, 40 ml water and 120 ml ethanol) and a second solution (4.2 g picric acid, 10 ml acetic acid, 70 ml ethanol and 10 ml water). The grain sizes were evaluated by line intercept method in the macrostructure using an image processing software (image pro plus 6.0) and the averages of Vickers hardness were estimated from 10 indentations measured using a 300 g load and a dwell of 15 s.

The phases identification was analyzed by X-ray diffraction using Cu K$\alpha$ radiation and the (0002), $(10\bar{1}0)$, $(11\bar{2}0)$ and $(10\bar{1}1)$ experimental pole figures were collected by a Rigaku's X-ray diffractometer equipped with a goniometer, using CrK$\alpha_1$ radiation. The pole figure intensities were normalized to units of multiples of a random distribution (MRD) and the orientation distribution functions (ODF) determined from them and represented in the Euler space ($0° \leq \varphi_1 \leq 90°$, $0° \leq \Phi \leq 90°$, $0° \varphi_2 \leq 60°$) in terms of $\varphi_2$-sections, using MTEX, a texture analysis software program [14]. The sample symmetry was considered orthorhombic, including the following reference directions: $<1\bar{2}10>$ rolling direction (RD), $<10\bar{1}0>$ transverse direction (TD) and $\langle 0001 \rangle$ normal direction (ND).

## 2. Results and discussion

### 2.1. Microstructure

The commercial twin roll-caster magnesium alloy sheet (the as-received material) exhibited an initial microstructure that consisted of equiaxed-grains with an average grain size of $13 \pm 3$ μm (Fig. 1), which can be an indication of recrystallized state of as-received material and supported by its low Vickers hardness value ($50 \pm 2$ HV). The initial microstructure of the AZ31B magnesium alloy consists of $\alpha$-Mg and few eutectic phases ($Mg_2Al_3$, $Al_8Mn_5$, $Al_4Mn$ and AlMn) distributed heterogeneously in the magnesium matrix. The morphology of eutectic precipitates varied from blocky structures (~6 μm) to fine particles, their EDX analyses showed Al and Mn as their majority elements (Fig. 1b), what means that the alloying elements of AZ31B magnesium alloys precipitated, during the twin-roll casting process, as secondary-phases containing mainly aluminum and manganese [3]. The combination of solidification and rolling during twin roll caster processes usually promote the formation of segregations and brittle precipitates, which cannot be completely suppressed on magnesium alloys containing aluminum and zinc [15]. In order to reduce them, suitable heat treatments are required to dissolve or distribute them uniformly; however, in this work the cross rolling experiences were applied directly on samples in as-received state.

During cross-rolling, significant microstructural changes were generated on the initial microstructure of AZ31B magnesium alloy, which were remarkably affected by the deformation degree and rolling temperature. The main microstructures generated for different deformation conditions can be seen in the Fig. 2. Cross-rolling experiences at low temperatures (25 °C and 100 °C) generated microstructures with some regions of small grains relatively undeformed (~7 μm) surrounded by bigger deformed grains, wherein mechanical twins were preferentially formed and intensified when the deformation degree increased. Pointing out that the maximum thickness reduction (between 15% and 20%) reached by cold cross-rolling was higher than conventional cold rolling; this improvement resulted from the change of rolling direction, since it generated higher grain subdivision on different regions of deformed samples, probably involving geometrically necessary boundaries (GNBs) and slip-induced grain boundary sliding (GBS) during the grain subdivision mechanisms, which are commonly originated in inhomogeneous plastic deformations of polycrystalline materials with high anisotropy levels such as magnesium alloys [22,9]. However, a massive

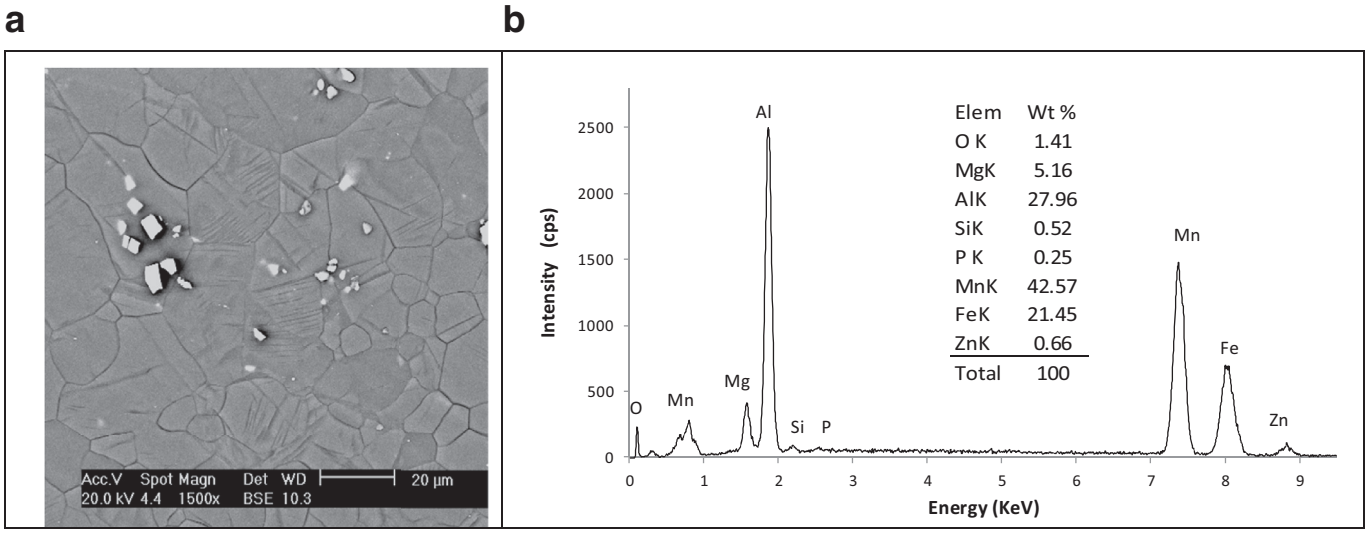


Fig. 1. (a) SEM-Microstructure of twin roll-caster AZ31 magnesium alloy sheet and (b) EDX analysis spectrum of second phase precipitates.

formation of mechanical twins in combination with conjugated shear bands is often associated with sudden failures, specially generated on conventional cold rolling samples deformed with reductions higher than 10%, a massive twin-boundary interaction generates double-twin formation and increases the localized stress concentration, the strain hardening and the anisotropy level [16].

Increasing the rolling temperature to 200 °C, the microstructure of warm cross-rolled specimens consisted of coarse grains slightly elongated along the rolling direction, wherein massive mechanical twins were formed in multiple parallel and cross-bonded twin boundary groups. No evident recrystallized grains were observed, although the rolling temperature was close to the recrystallization temperature (> 0.5 Tm, Tm: the absolute melting temperature). However, above 200 °C, fine recrystallized grains were evidenced in some regions, especially when the rolling reduction was higher than 10%, then deformation degrees close to 0.16 = Ɛ were enough to reduce the driving force required to nucleate new grains during the warm cross rolling at 250 °C of AZ31B magnesium alloy. The recrystallized grains were formed mainly along the shear bands and mechanical twins because high plastic deformations are concentrated on them. The deformation mechanism during warm cross-rolling essentially included basal and non-basal slips, mechanical twins and shear band formations, which were developed simultaneously with dynamic recrystallization, generating heterogeneous microstructures with coarse deformed grains (>16 μm) partially elongated along the rolling direction and fine grains (<6 μm) free of mechanical twins. The dynamic recrystallization was enhanced notably at temperatures higher than 250 °C by the increase in Mg-atom diffusion and by the reduction of driving forces required for nucleation. The massive cross-slips and grain boundary migrations on mechanical twins and shear band promoted the nucleation and nucleus growth. The uneven rates of recrystallization generated inhomogeneous microstructures with evident grain refinement in determined regions of warm cross-rolling samples, wherein fine grains were probably directly developed from transformation of sub-grains into high angle grain boundaries on twin-twin intersections, since cross-twinning boundary processes facilitate the formation of new grains during recrystallization [17,18].

### 2.2. Vickers hardness

According to the maximum thickness reduction achieved in a single pass at each temperature of cross-rolling experiences (Table 2), the change in rolling direction had a positive impact on the elongation of the AZ31 magnesium alloy sheet compared to conventional unidirectional rolling processes. Cold rolling samples achieved an upper limit of deformation ($\varepsilon = 0.16$) applying 15% thickness reduction in a single pass, higher reductions fractured the sample into many small pieces due to the high anisotropy and heterogeneous strengthening associated to the massive twin–twin interactions and the creation of barriers to the dislocation propagation that produce together twinning-induced hardening.

At 200 °C, the AZ31 magnesium alloy still exhibited low ductility during warm cross rolling; the maximum rolling reduction prior to edge cracking (samples without evident side-cracks) was the same as that of the cold cross-rolled samples. However, increasing the rolling temperature to 250 °C, it was evidenced a gradual increase in elongation up to 25% as a result of the activation of different deformation modes. Higher reductions were disregarded due to the presence of small edge-cracks, even though only scarce cracks were evidenced on their lateral sides. In the case of the warm cross rolling experiences developed at 300 °C, the upper limit of deformation ($\varepsilon = 0.51$) was achieved by applying reductions of 40% in a single pass.

The variation of Vickers hardness as a function of the rolling reduction is shown in Fig. 3, where it is observed the considerable strengthened of as-received material after cold

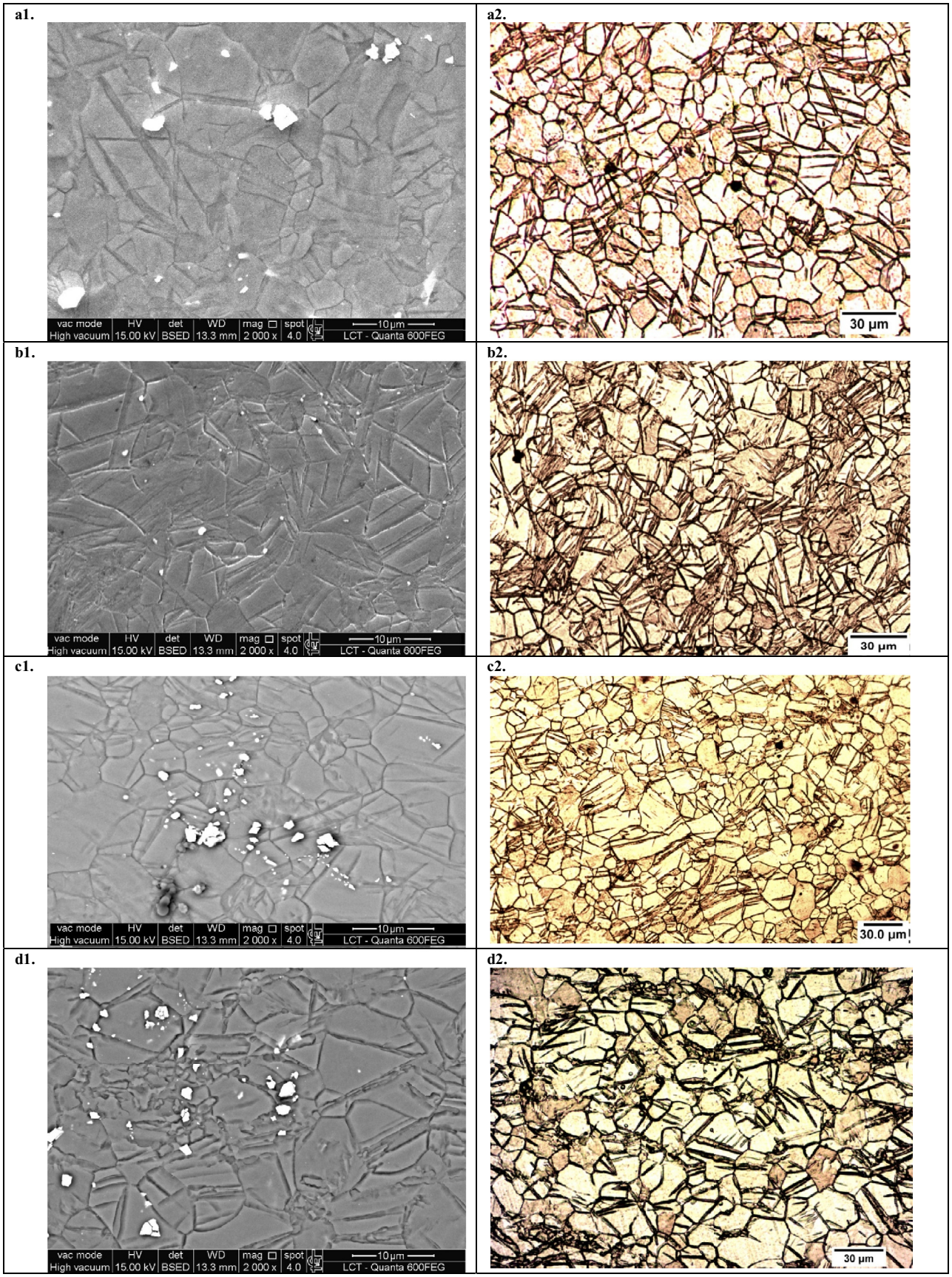


Fig. 2. Microstructures of cross-rolling samples deformed by: ($a_1$, $a_2$) 15% rolling reduction at 25 °C; ($b_1$,$b_2$) 15% rolling reduction at 200 °C; ($c_1$,$c_2$) 20% rolling reduction at 250 °C; ($d_1$,$d_2$) 40% rolling reduction at 300 °C.

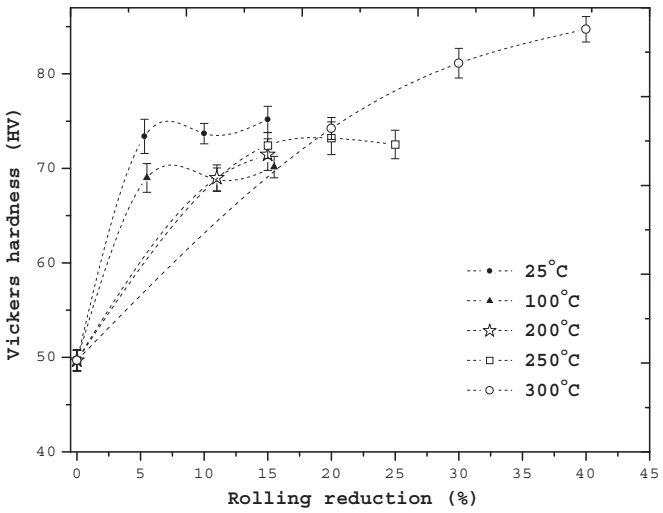


Fig. 3. The variation of Vickers hardness as a function of the thickness reduction applied during the cross-rolling experiences.

cross-rolling at room temperature. The hardness of cold cross-rolled samples increased from 50 ± 2 HV to 75 ± 2 HV by applying low thickness reductions (≤15%), this strengthening was mainly influenced by the rolling reduction and generated by the activation of various deformation mechanisms, including mechanical twins, slip on basal and non-basal planes and high dislocation pile–ups produced at grain and small particle boundaries of cold cross-rolled magnesium samples of AZ31. However, at 100 °C and 200 °C, the hardness increase was slightly reduced (~70 HV) compared with the samples deformed at room temperature. Such hardness reduction can be attributed to the dynamic recovery that certainly occurred at those temperatures, since, it was reported that the stress necessary to induce cross slips starts to decrease at 100 °C and the stacking fault energy (SFE) controls the occurrence of dynamic recovery and recrystallization, the high SFE of magnesium alloys facilitates the dynamic recovery during thermo-mechanical processes, increasing cross-slips and the dislocation annihilations which promote the softening mechanisms of recovery [19].

Increasing the rolling temperature to 250 °C or 300 °C, the work hardening should, in theory, have decreased due to the high activity of non-basal slips, which intensify the dislocation annihilation and the dynamic recrystallization, which in turn reduce the Vickers hardness values; however, instead of decreasing, their values increased at similar levels or higher than cold cross-rolled samples deformed at room temperature, this was attributed to the effects of segregations and precipitates of secondary phases, type of mechanical twins, grain size refinement generated at high temperatures and solid-solution strengthening that results from solutes dissolved into Mg, introducing distortion of lattice that can hinder the glide of dislocations and improve the cross-slips [20].

### 2.3. X-ray diffraction

Fig. 4 displays the X-ray diffraction patterns of the AZ31B magnesium alloy in as-received state and after cross-rolling. It was selected experiences developed under more representative conditions of cold and warm cross-rolling. Their strongest diffraction lines of as-received material coincided with those of $\alpha$-Mg (ICSD: 89-4894), confirming that the majority phase

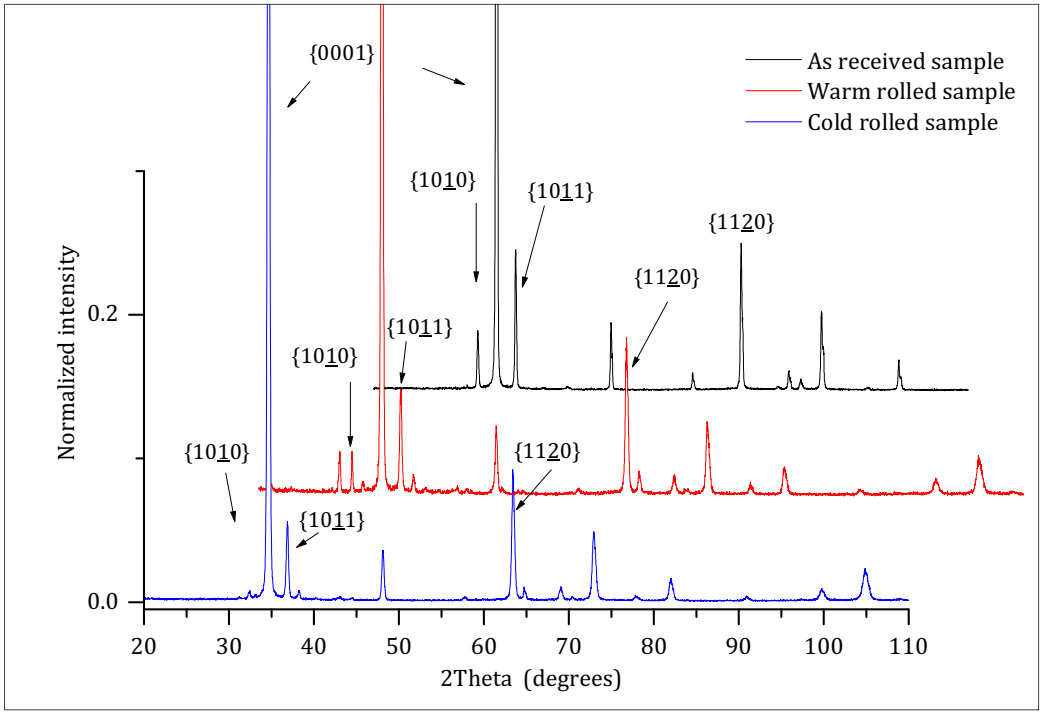


Fig. 4. X-ray diffraction spectra of as-receive material and cross-rolling samples deformed with 15% thickness reduction at 25 °C and 250 °C.

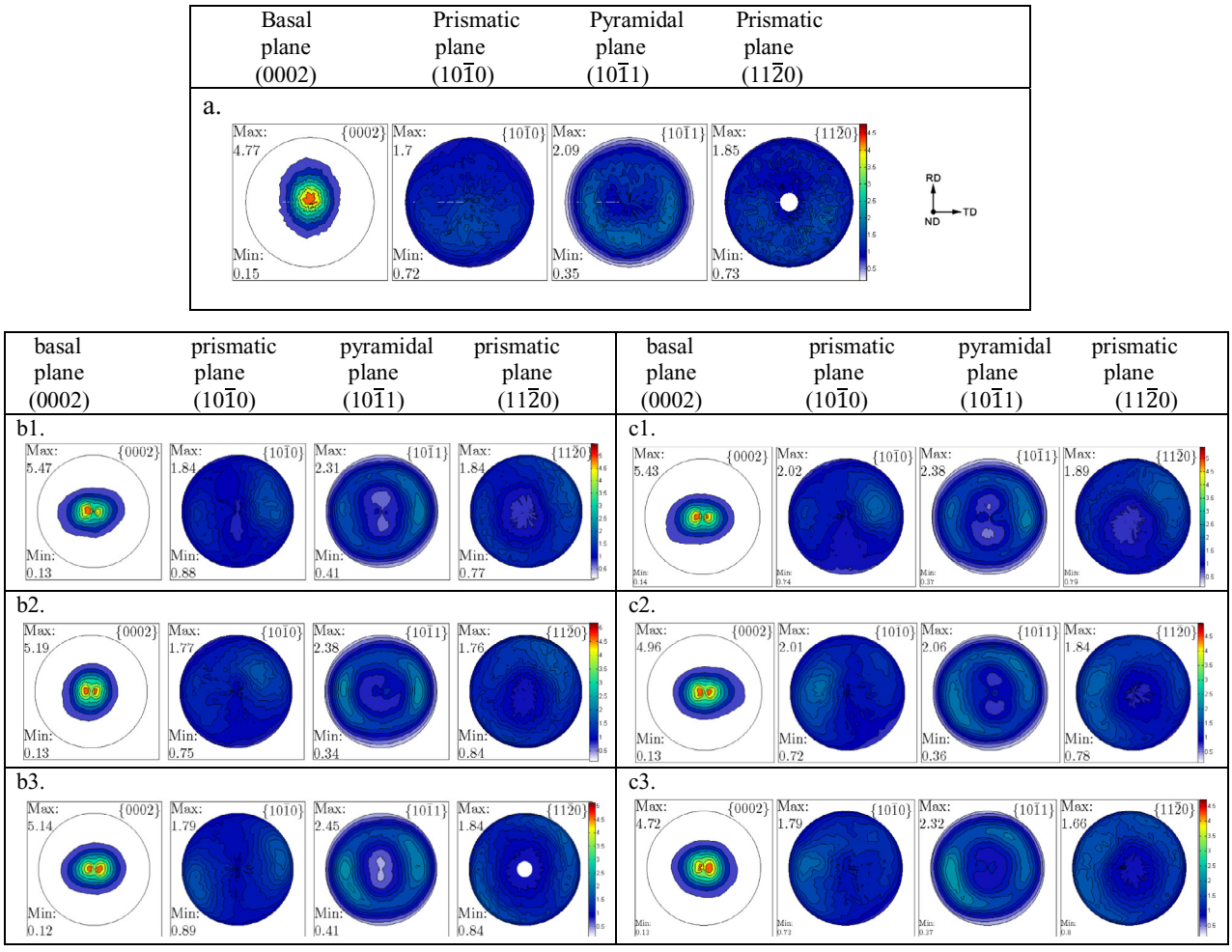


Fig. 5. Pole figures of AZ31magnesium alloy in (a) as-received state and after cold cross-rolling experiences, deformed by different rolling reductions (b1) 5%, 25 °C, (b2) 10%, 25 °C, (b3) 15%, 25 °C, (c1) 5%, 100 °C, (c2) 10%, 100 °C and (c3) 15%, 100 °C.

correspond to $\alpha$-Mg and most of its alloying elements are in solid solution. After cross- rolling experiences, notable changes in peak intensities were observed due to deformed texture and high plastic anisotropy of AZ31B magnesium alloys, moreover, slightly changes in peak position were developed causing a misfit in the phase peaks and affecting the grain lattices.

The presence of intermetallic phases was not possible to detect in both as-received material and cold-rolled samples by the X-ray diffraction technique due to their heterogeneous distribution and reduced quantities, it is known that the intensity of the measured diffraction peak is directly proportional to the volume of the diffracting grains. However, the diffraction patterns of warm cross-rolled samples deformed over 200 °C evidenced small new diffraction lines at $2\theta = 27°$, 30°, 43°, 66°, 78° and 95°, which are related to the intermetallic phases: Al8Mn5 (ICSD-65-6848), Al3.16Mg1.84 (ICSD-65-6848), Mg0.97Zn0.03 (ICSD 65-4596). This appears to the volume fraction of second phase particles increased during warm cross-rolling due to greater diffusion of Al and Mn atoms in the magnesium matrix.

The high peak of basal line intensities at $2\theta = 35°$ observed on cold cross-rolling samples denote that the intense activity of basal slips intensified the basal texture at low temperatures, while during warm cross-rolling, the activity of (10$\bar{1}$1) pyramidal planes introduced considerable increases on their diffraction intensities, denoting that some of them were favorable rotated to the rolling plane.

### 2.4. Texture analysis

The experimental (0002), (10$\bar{1}$0), (11$\bar{2}$0) and (10$\bar{1}$1) pole figures collected from the rolling surface of specimens are shown in Figs. 5 and 6, in which it is possible to see the texture evolution of cross-rolling experiences developed under different conditions. The main texture is easily visible through pole figure intensity, which is strongly related with a deformation mode and its influence on the deformation mechanism. The intense basal pole figure of the as-received material reflects a strong basal texture represented by a single-peak basal pole figure almost fully aligned with the normal direction (ND), showing that most basal planes are lying parallel

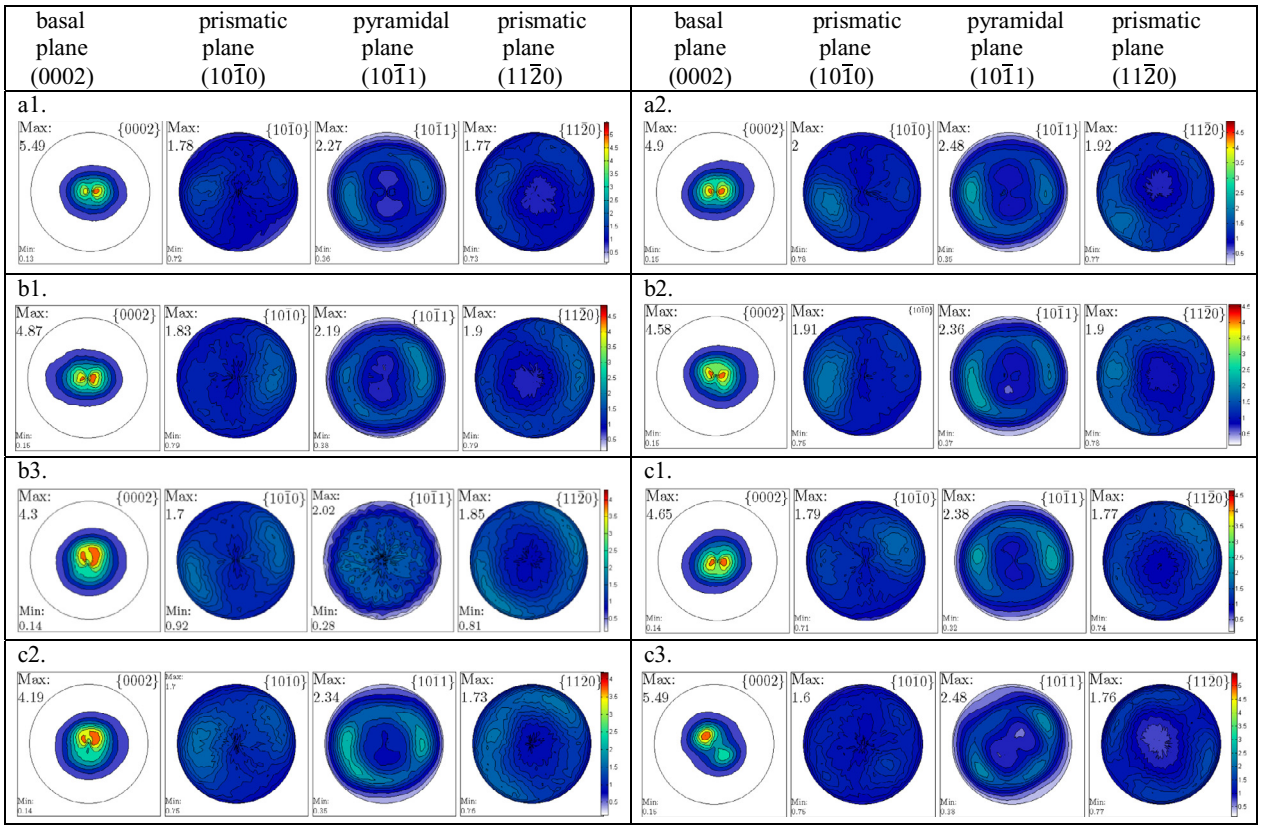


Fig. 6. Pole figures of AZ31magnesium alloy after warm cross-rolling experiences, deformed by different rolling reductions of (a1) 10%, 200 °C, (a2) 15%, 200 °C, (b1) 15%, 250 °C (b2) 20%, 250 °C, (b3) 25%, 250 °C (c1) 20%, 300 °C, (c2) 30%, 300 °C and (c3) 40%, 300 °C.

to the rolling direction (RD) with their *c*-axes aligned parallel to ND.

It is often suggested that Mg-alloys develop an ideal basal texture, since they have a nearly ideal *c*/*a* ratio of 1.624. However, this texture is rarely observed because the pole symmetry is not totally radial or collinear with the ND. Normally, the basal pole intensity is spread toward the RD and tilted away from ND by ± 10°, showing a slightly off-basal texture, as is shown in this case. The as-received material showed a typical basal texture of AZ31B magnesium alloy in a recrystallized state, showing a single intensity maximum almost centered at the ND and a basal pole spreading towards the rolling direction promoted by alloying elements.

After cross-rolling experiences, in some cases, the initial basal texture was weakening or strengthening depending mainly on the rolling temperature and deformation degree, which can activate simultaneously different deformation mechanisms and the dynamic recrystallization. The maximum intensity of basal pole figures of deformed samples were represented by double-peaks with different intensities, revealing that the initial distributions of the basal planes, represented by a strong single-peak pole figure, was divided into two groups that are spreading along the TD and tilted away from the normal direction with opposite orientations (∼ ± 10°). This splitting of basal pole figures was also reported in some studies of wrought magnesium alloys and it was attributed to the massive formations of shear bands and mechanical twins during deformations [12]. According Yi et al, the phenomenon of basal-pole splitting is mainly attributed to the formation of {10$\bar{1}$1} compression twinning followed by {10$\bar{1}$2}re-twinning (secondary twins), which are activated only in grains whose c-axis are tilted by more than 30° away from the ND. However, the activation of tensile twins is quickly developed in grains with their *c*-axis tilted away no more than 45° with the ND because their CRSS values are the lowest lower [21]. Normally, in conventional unidirectional rolling processes, the spreading of basal pole figures along the rolling direction is explained as being promoted by extension twins. However, in these cross rolling processes, it is important to point out that the last transverse direction was previously the rolling direction prior to deformations. It is known that a change in rolling direction affects the texture evolution, but it is necessary a certain deformation stress to rotate all basal planes through the new rolling direction. Therefore, it is very likely that each deformation stress applied during cross-rolling experiences was not sufficient to develop significantly basal plane rotations, and consequently part of basal pole distribution still evidenced a scatter along the transverse direction.

The basal texture strengthening produced during cold cross-rolling was a result of deformation mechanisms activated at low temperatures, such as mechanical twinning and basal plane slips. The rolling reduction increases generated lower increases in intensities registered by their double-peak basal pole figures (Fig. 7). This behavior can be at-

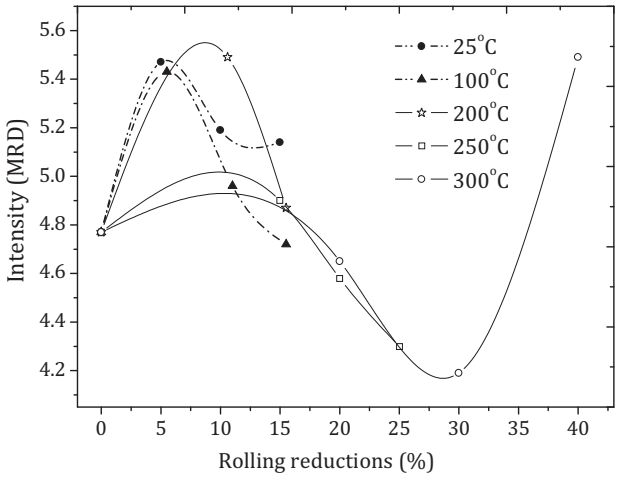


Fig. 7. Variation of the texture intensity as a function of the thickness reduction applied during the cross-rolling experiences.

tributed to the change of rolling direction, which promoted a greater spreading of basal pole figures, contrary to conventional rolling, in which the intensity of basal pole figures commonly increases with an increase in the rolling reduction. At 100 °C, the increase of basal texture intensity was more limited increasing the rolling reduction. The rolling reduction of 15% generated a basal texture intensity lower than that of as-received material (Fig. 7).

Warm cross-rolling carried out at 200 °C, with thickness reductions of 10% still generated a strong basal textures with intensity higher than those evidenced in cold rolling samples (Fig. 6). However, at 250 °C and 300 °C, rolling reductions between 20% and 30% weakened notably the initial basal texture generating more asymmetric basal pole figures, one of their double basal pole peaks rotated along the RD, forming small angles with the ND, between 15° to 30°. This rotation indicates that some non-basal texture components were generated as a result of the interaction of non-basal slips with massive twinning formation, which reorientations shift the non-basal planes to favorable positions to promote their slips.

The formation of double-peak basal pole figures during warm cross rolling was mainly develop by the secondary-twins, and by the notable increase in the activity of $<c+a>$ pyramidal slip, rather than prismatic slip [26,27]. According to the intensity variation of basal pole figures as a function of reduction in thickness (Fig. 7), it can be noted that the texture intensity of as-received material began to be weaken when the rolling reduction exceeded 15% at low temperatures of cold cross-rolling or by the increase of rolling temperature, above 200 °C. This basal texture weakening is the most representative feature of warm cross-rolling, however reductions higher than 30% at 300 °C strengthened again the initial basal texture, demonstrating that the basal slips and mechanical twins had intense activities at high strains, transferring the basal texture again, via static recrystallization during the sample cooling [22].

The crystallographic texture evolution was also analyzed in terms of the orientation distribution function (ODF) calculated from the experimental pole figures. The ODF functions represented in a three-dimensional space have their crystallographic orientations defined by Euler angles ($\varphi_1$, $\Phi$, $\varphi_2$) or Miller–Bravais indices $\{hkil\}<uvtw>$, this last one is the most used, where a groups of grains that exhibits their $\{hkil\}$ planes parallel to the rolling surface and their $\langle uvtw\rangle$ directions parallel to the rolling direction is represented by their $\{hkil\}\langle uvtw\rangle$ indices. All intensities depend on the number of grains with the same orientation [23]. For magnesium alloy sheets, the Euler space is restricted to a small region ($0°\leq\varphi_1\leq 90°$, $0°\leq\Phi\leq 90°$ and $0°\leq\varphi_2\leq 60°$) as a consequence of crystal structure and sample symmetry. On the other hand, it is commonly represented in two-dimensional sections, slicing the Euler space into parallel two-dimensional sections, maintaining one angle constant. If the $\varphi_1$-angle is kept constant, the $\varphi_1$-sections display the sample directions relative to the crystal axes; in contrast, when the $\varphi_2$-angle is fixed, the $\varphi_2$-sections display the crystal directions relative to the sample axes [24]. The main texture components of magnesium alloy sheets are easily visualized in $\varphi_2$-sections at $\varphi_2=0°$ and $\varphi_2=30°$, the ideal positions of basal texture components are schematically represented in the Fig. 8, this representation was developed considering the crystal directions ($[2\bar{1}\bar{1}0]$, $[10\bar{1}0]$ and [0001]) parallel to the sample references (RD, TD and ND), respectively. When the basal planes lie parallel to the rolling surface and their $<2\bar{1}\bar{1}0>$ crystal directions are aligned parallel to the RD, the basal texture is represented by $(0001)<2\bar{1}\bar{1}0>$, whereas the basal textures represented by $(0001)<10\bar{1}0>$ have their $<10\bar{1}0>$ crystal directions parallel to the RD. Each basal texture simultaneously generates two components in each $\varphi_2$-section, such as the $(0001)<2\bar{1}\bar{1}0>$ texture displays four components at (30°, 0°, 0°), (90°, 0°, 0°), (0°, 0°, 30°) and (60°, 0°, 30°). If the texture components present a dislocation towards the $\Phi$-angle, it means that basal planes are tilted away from the ND, for instance, the texture component at (0°, 20°, 0°) denotes that the basal planes are tilted 20° away from the ND with a distribution spread toward the TD, whereas an orientation at (90°, 20°, 0°) describes basal planes with a spreading along the RD [25].

According to the ODF of as-received material (Fig. 9), the initial texture was a partial basal fiber extended along the $\varphi_1$-angle (0–90°), displaying its main components close to ideal position of a basal texture represented by $\{0001\}<2\bar{1}\bar{1}0>$, revealing that most of basal planes lie parallel to the RD with their $<2\bar{1}\bar{1}0>$ directions aligned parallel to the RD. This texture is typically exhibited in twin roll-caster magnesium sheets. The fiber spreading along the $\Phi$-angle means that some basal planes are tilted away from the ND ($\leq 30°$), forming weak fibers such as the $\{1\bar{2}\bar{1}7\}$ fiber at $\Phi=10°$ and the $\{\bar{1}2\bar{1}5\}$ fiber at $\Phi=30°$ However, the fibers close to $\Phi=30°$ and the $\{1\bar{2}10\}$ fiber, formed at the bottom of the $\varphi_2$-sections, can be disregarded due to their low intensities.

The ODFs of cold cross-rolled samples (Fig. 10) confirmed that the initial basal texture was reinforced during deforma-

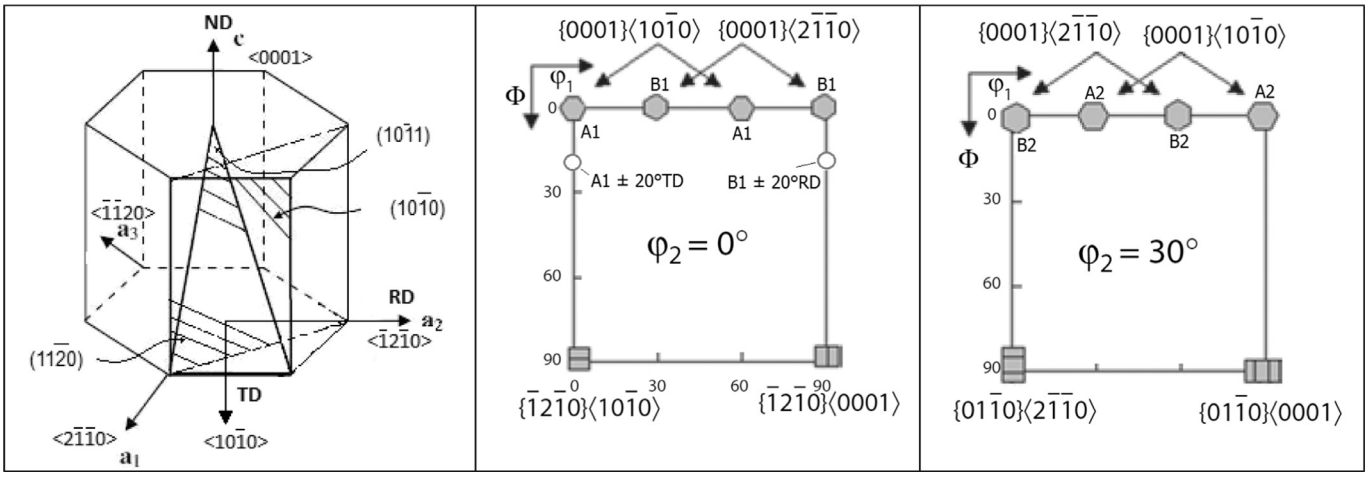


Fig. 8. Ideal positions of basal texture components represented in terms of ODF sections for $\varphi_2 = 0°$ and 30° sections [27].

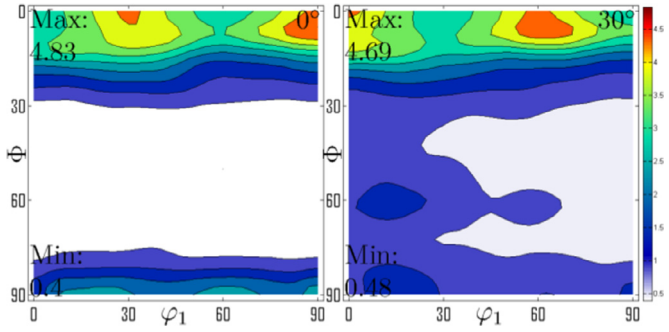


Fig. 9. The ODF ($\varphi_2$-sections: $\varphi_2 = 0°$ and $\varphi_2 = 30°$) of the AZ31B magnesium alloy sheet in as-received state.

tion, since their fiber components became more intense and spread out than those of the as-received material, in particular those components displayed at (30°, 0°, 0°) and (0°, 0°, 30°), which scattered across the Φ-angle when the thickness reduction increased to 15%. Furthermore, the fiber spreading increased more along the RD, almost reaching the {10$\bar{1}$7} fiber at $\Phi = 40°$, it shows that some basal planes were strongly rotated from the TD to the new RD. The variation in fiber intensity along $\varphi_1$, Φ, or $\varphi_2$ can give an idea about the texture changes in the deformed material as a function of deformation degree, therefore, vertical cuts along Φ-angles at (30°, 0°–90°, 0°) and horizontal cuts along $\varphi_1$-angles at (0°–90°, 10°, 0°) were developed for all ODF functions. The cut positions were selected on the maximum intensity of components that showed greater changes related with their spreading. The intensity distributions through the Φ-angles and $\varphi_1$-angles (Fig. 11) showed that only one basal fiber component in each section was reinforced during cold cross-rolling, in contrast to other one that exhibited a decrease. Cross-rolling at room temperature generated a great intensity on the basal fiber component at $\Phi = 12°$ and $\varphi_1 = 30°$. When the rolling temperature was increased to 100 °C, this component still concentrated high intensity at $\varphi_1 = 30°$, albeit a new weak basal fiber component appeared at $\varphi_1$-angle at 10° as a result of

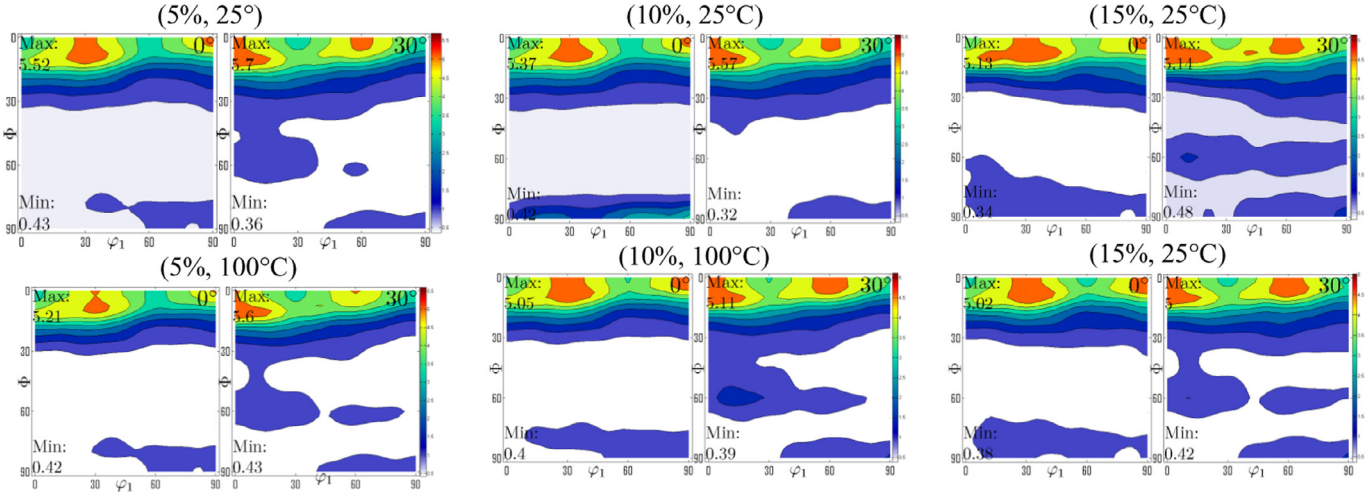


Fig. 10. The ODF ($\varphi_2$-sections: $\varphi_2 = 0°$ and $\varphi_2 = 30°$) of the AZ31B magnesium alloy after cold cross rolling experiences at 25 °C and 100 °C.

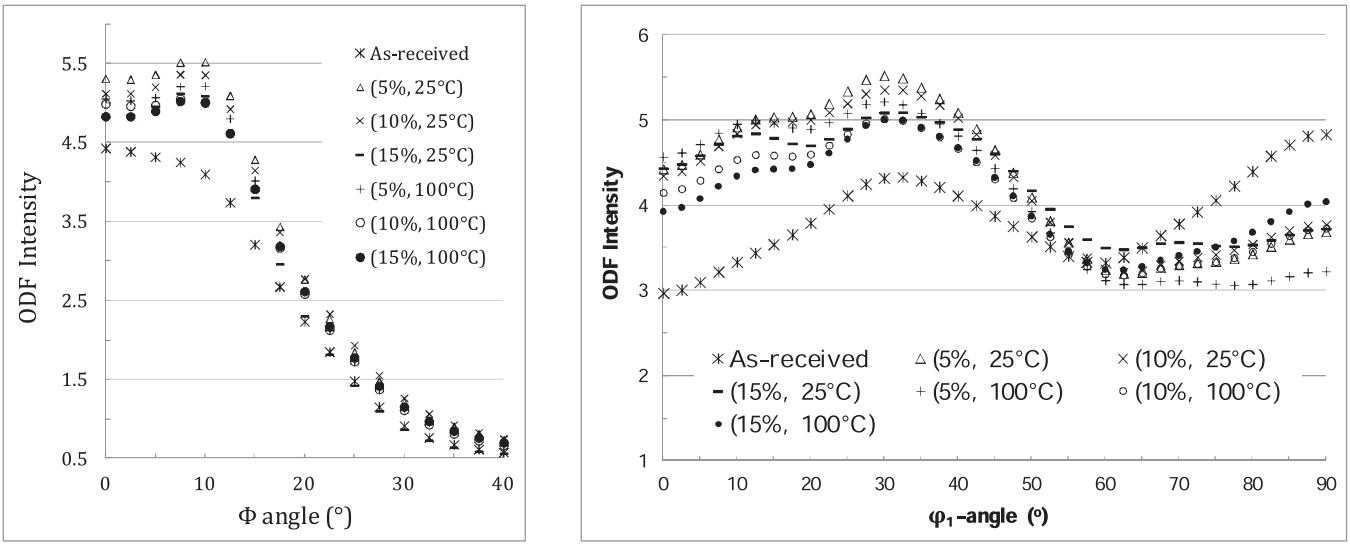


Fig. 11. Vertical and horizontal cuts along {30°,0°–90°,0°} and {0°–90°,10°,0°} of the $\varphi_2$-sections, showing the intensity distributions across Φ-angle and $\varphi_1$-angle of the as-received material and cold cross-rolling samples.

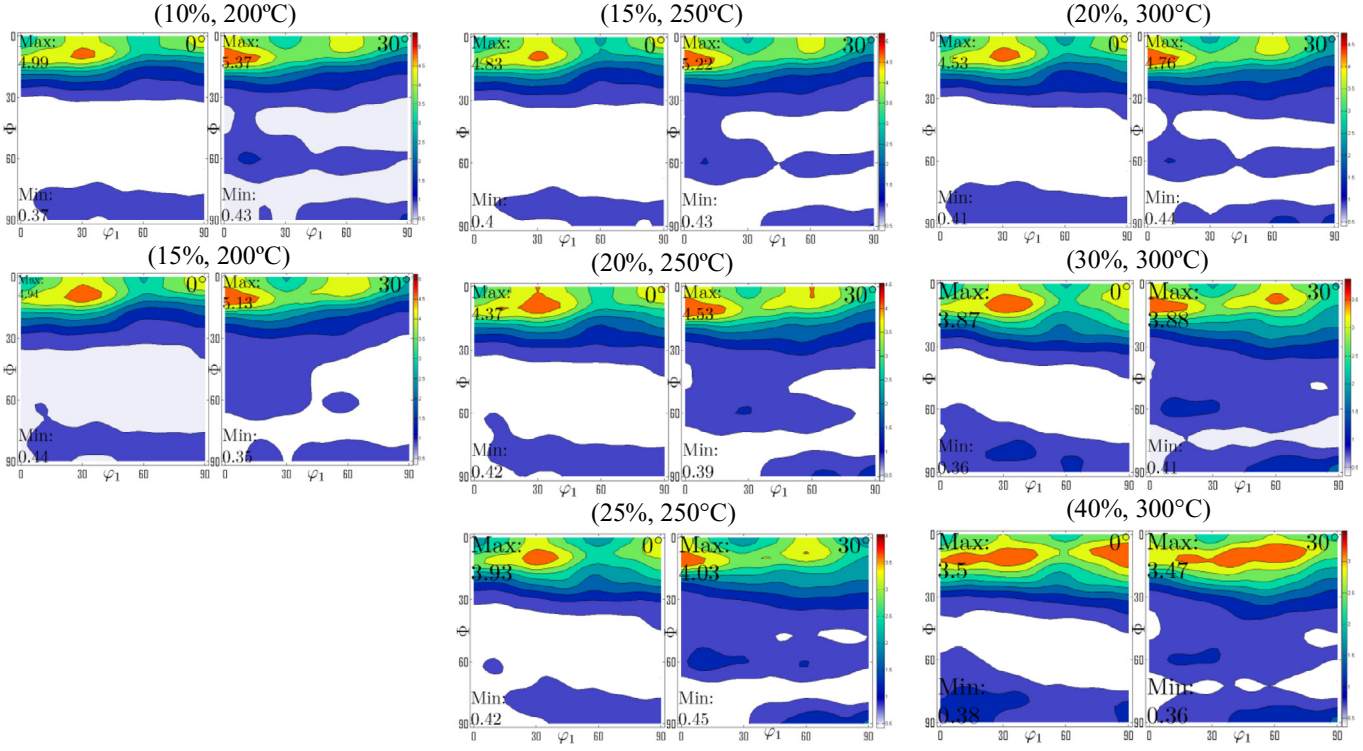


Fig. 12. The ODF ($\varphi_2$-sections: $\varphi_2 = 0°$ and $\varphi_2 = 30°$) of the AZ31B magnesium alloy after warm cross rolling experiences at 200 °C and 250 °C.

mechanical twins and basal plane rotations generated by high plastic strains.

The ODF functions of warm cross-rolled samples (Fig. 12) exhibited basal fibers dislocated through the Φ-angle, achieving new positions between 15° and 35°; however, their main texture can still be represented as a basal partial fiber represented by $\{0001\}<2\bar{1}\bar{1}0>$. At 200 °C and 250 °C, low deformation degree ($\leq 0.15$) intensified the initial basal fiber and dislocated it through the Φ-angle. However, higher reductions weakened the initial texture, exhibiting basal fibers with lower intensities than the as-received material. It is also interesting to note that a new fiber component was generated at $\varphi_1 = 10°$ in conjunction with the main $\{0001\}<2\bar{1}\bar{1}0>$ component at $\varphi_1 = 30°$, spreading more the latter through the $\varphi_1$-angle. This new texture component represented by $\{0001\}<10\bar{1}0>$ became more evident at high temperatures ($\geq 250$ °C) demonstrating that the interaction of non-basal slips and mechanical twins with dynamic re-

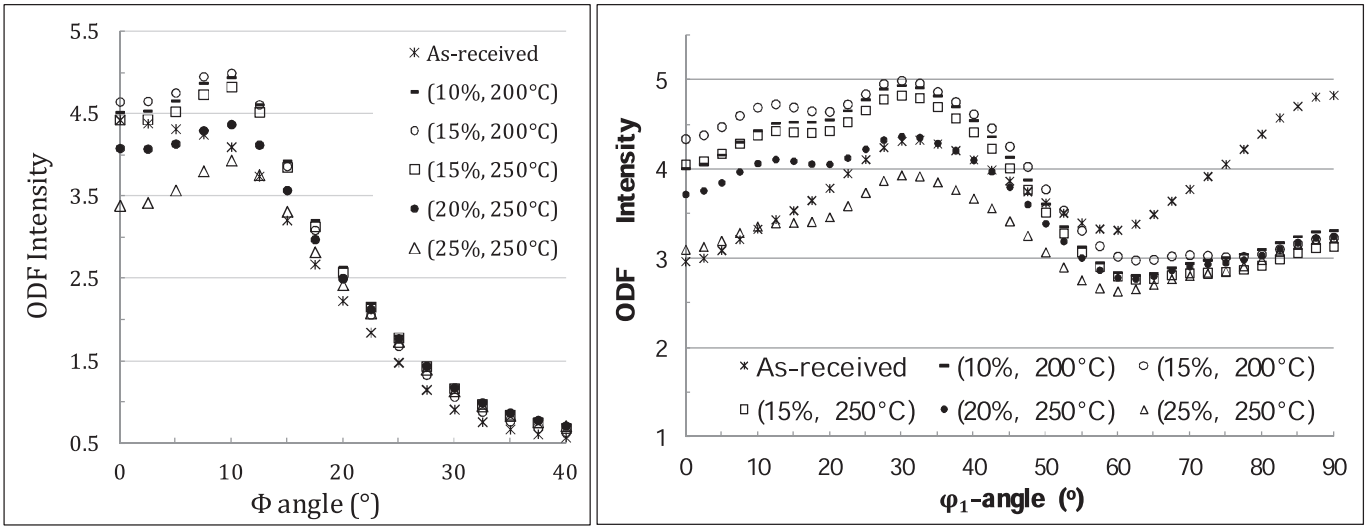


Fig. 13. Vertical and horizontal cuts along {30°,0°–90°,0°} and {0°–90°,10°,0°} of the $\varphi_2$-sections, showing the intensity distributions across Φ-angle and $\varphi_1$-angle of the as-received material and warm cross-rolling samples deformed at 200 °C and 250 °C.

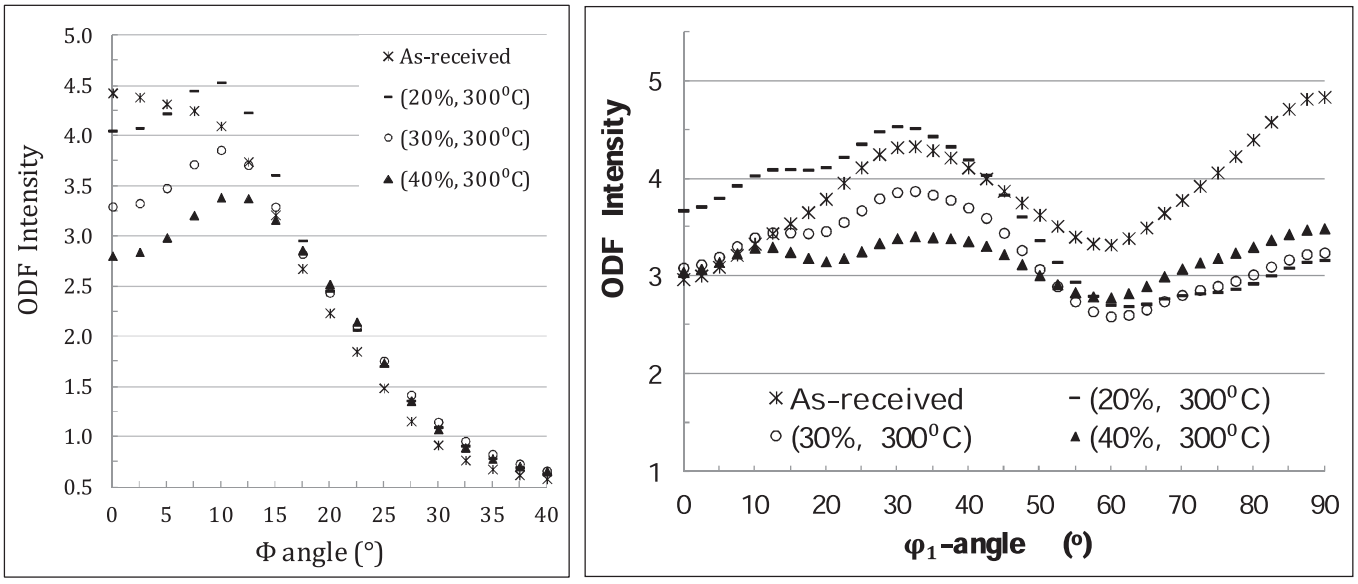


Fig. 14. Vertical and horizontal cuts along {30°,0°–90°,0°} and {0°–90°,10°,0°} of the $\varphi_2$-sections, showing the intensity distributions across Φ-angle and $\varphi_1$-angle of the as-received material and warm cross-rolling samples deformed at 300 °C.

crystallization contributed to the weakening of initial basal texture. The intensity distributions through the Φ-angles and $\varphi_1$-angles (Fig. 13) confirmed that high thickness reductions can weaken the basal texture, especially around the component at $\varphi_1 = 30°$, which evolved in positions during warm cross-rolling at 300 °C from $\phi = 0°$ (in as-received state) to $\phi = 12°$ while the component spreading at $\varphi_1 = 90°$ was severely reduced without showing displacement across the Φ-angle. The new shifted fiber can be represented by $\{10\bar{1}9\}$ fiber, which presented two components around the (0°, 0°, 0°) and (30°, 0°, 30°) positions, and represented by the $(0001) < 10\bar{1}0 >$ texture. The weak $\{01\bar{1}0\}$ fiber in the lower part of the $\varphi_2$-sections can be disregarded due to low intensity. In this sense, the texture of warm cross-rolling samples resulted from a combination of two types of crystallographic orientation: ($\{0001\} < 21\bar{1}0 >$ and $\{0001\}\langle 10\bar{1}0\rangle$) generated simultaneous by the interaction of deformation mechanism and dynamic recrystallization. The mechanical twins and non-basal slips, such as the $(10\bar{1}0)[\bar{1}210]$ prismatic slips and the $(10\bar{1}1)[\bar{1}210]$ pyramidal slips activated at temperatures above 200 °C, contributed significantly to the weakening of the initial basal texture, generating new texture components and spreading more the basal fiber along the RD.

## 3. Conclusions

The cross-rolling of AZ31B magnesium alloy plate generated microstructures dependent mainly on the deformation degree and rolling temperature, and basal textures determined mainly by deformation mechanisms activated dur-

ing the cross-rolling and influenced by the initial texture and rolling direction.

Low strain rates generated heterogeneous microstructures with regions of small untwined grains surrounded by coarse twinned grains and shear-bands, while high strain rates enhanced the twinning and shear band formations, even at high rolling temperatures when the dynamic recrystallization was developed in conjunction with the thermally active deformation mechanisms. On the other hand, the sudden failures during cold cross-rolling with reductions higher than 15% were associated with the massive formation of shear bands conjugated with mechanical twins, whereas, at temperatures over 200 °C the same features enhanced the dynamic recrystallization that improved the ductility. However, eutectic precipitates influenced on the deformability behavior and hardening evolution during warm cross-rolling.

The initial basal texture was successfully weakened by cross-rolling when it was carried out with thickness reductions higher than 15% and rolling temperatures over recrystallization temperature of AZ31B magnesium alloy (over 200 °C), showing as a final texture a combination of two types of crystallographic orientation ($\{0001\}<2\bar{1}\bar{1}0>$ and $\{0001\}\langle 10\bar{1}0\rangle$) generated by the combination of deformed and dynamically recrystallized grains. Whereas, the final texture of cold cross-rolling samples was still represented by the initial texture ($\{0001\}<2\bar{1}\bar{1}0>$) because their low strain rates strengthened the initial basal texture, in contrast to that observed at high rolling temperatures.

## Acknowledgment

The present research was supported by CAPES-(Coordenação de Aperfeiçoamento de Pessoal de Nível Superior), process no. PNPD20130250 - 22001018034P4.

## References

[1] M.M. Avedesian, H Baker, Magnesium and Magnesium Alloys, ASM International, 1999 s.l 978-0-87170-657-7.
[2] B.L. Mordike, T. Ebert, Mater. Sci. Eng. A302 (2001) 37–45.
[3] H. Watari, K. Davey, M.T. Alonso Rasgado, T. Haga, S. Izawa, in: Proceedings of the Advances in Materials and and Processing Technologies, 2003, pp. 720–723.
[4] T. Sakai, H. Utsunomiya, H. Koh, Mater. Sci. Forum 539–543 (2006) 3359–3364.
[5] S.R. Agnew, O. Duygulu, Int. J. Plast. 21 (2005) 1161–1193.
[6] C.N. Tome, W.R. Blumenthal, M.A.M. Bourke, D.W. Brown, G.C. Kaschner, P. Rangaswamy, Mater. Sci. Forum. 408–412 (2002) 263–268.
[7] J. Koikea, T. Kobayashia, T. Mukaib, H. Watanabeb, M. Suzukia, K. Maruyamaa, K. Higashic, Acta Mater. 51 (2003) 2055–2065.
[8] M. Sanjari, S. Tamimi, J. Su, A.S. Kabir, K. Hara, H. Utsunomiya, L. Kestens, Mater. Sci. Eng 91 (2014), doi:10.1088/1757-899X/82/1/012030.
[9] J. Koike, R. Ohyama, T. Kobayashi, M. Suzuki, K. Maruyama, Mater. Trans. 44 (2003) 445–451.
[10] Y. Pei, A. Godfrey, J. Jiang, Y. Zhang, W. Liu, Q. Liu, Mater. Sci. Eng. A: Struct. Mater.:Prop. Microstruct. Process. 550 (2012) 138–145.
[11] P Cizek, M.R Barnett, Scr. Mater. 59 (2008) 952–692.
[12] L. Jiang, J.J. Jonas, Scr. Mater 58 (2008) 803–806.
[13] X. Lia, T. Al-Sammana, G. Gottsteina, Mater. Design 32 (2011) 4385–4393.
[14] F. Bachmann, R Hielscher, H. Schaeben, Solid State Phenom. 160 (2010) 63–68.
[15] M. Ullmann, R. Kawalla, H.-P. Vogt, La Metal. Ital. (2014) 35–42. 3/2014 http://www.fracturae.com/index.php/aim/article/view/1387.
[16] Qin Yu, Jian Wang, Y. Jiang, R.J. McCabe, N. Li, C.N. Tome, Acta Mater 12 (2014) 28–42 77.
[17] H.Q. Sun, Y.N. Shi, M.X. Zhang, K. Lu, Acta Mater. 55 (2007) 975–982.
[18] J. Su, A.S.H. Kabir, M. Sanjari, I.-H. Jung, S. Yue. 2016, pp. 267–271. https://link.springer.com/chapter/10.1007%2F978-3-319-48114-2_53.
[19] K. Mdthís, Z. Trojonovd, P. Lukú, J. Lendvaí, Allum. E Leghe (2002) 33–36.
[20] J.A. Yasi, L.G. Hector Jr, D.R. Trinkle, Acta Mater. 58 (2010) 5704–5713.
[21] S. Yi, I. Schestakow, S. Zaefferer, Mater. Sci. Eng. A 516 (2009) 58–64.
[22] M. Haghshenas, V. Bhakhri, R. Oviasuyi, R.J. Klassen, MRS- Materials Research Society 5 (2015) 513–518.
[23] Y.N. Wang, J.C. Huang, Mater. Chem. Phys. 81 (2003) 11–26.
[24] O. Engler, V. Randle, Introduction to Texture Analysis: Macrotexture, Microtexture, and Orientation Mapping, CRC Press, 2009, p. 488. s.l.
[25] J. Hirsch, T. Al-Samman, Acta Materialia 61 (2013) 818–843.
[26] S.H. Park, et al., Scripta Mater. 28 (2010) 202–205 de 2 de.
[27] N. Stanford, M.R. Barnett, J. Alloys Compd. 466 (2008) 182–188.
[28] Y. Chino, K. Sassa, A. Kamiya, M. Mabuchi, Mater. Trans. 47 (2006) 2555–2560.